Applied Catalysis B: Environmental 337 (2023) 122978

Contents lists available at ScienceDirect

Applied Catalysis B: Environmental

journal homepage: www.elsevier.com/locate/apcatb

Ultra-low-loading Pd nanocrystals modified Ni foam electrode for efficient electrochemical hydrodechlorination

Huan Wu [a], Zhechuan Mao [a], Baoquan Liu [a], Deyin Chen [a], Meiqin Shi [a], Bosheng Lv [b], Yinghua Xu [a,*], Lianbang Wang [a]

[a] Petroleum and Chemical Industry Key Laboratory of Organic Electrochemical Synthesis, College of Chemical Engineering, Zhejiang University of Technology, Hangzhou 310014, PR China

[b] College of Environment, Zhejiang University of Technology, Hangzhou 310014, PR China

ARTICLE INFO

Keywords:
Dechlorination
Palladium
Chlorophenol
Low coordination
Catalytic site

ABSTRACT

Pd nanocrystals modified Ni foam electrode (Pd NCs/Ni) with Pd loading of 12.5 μg cm^{-2} was prepared via electrodeposition and exhibited higher mass activity in the electrochemical hydrodechlorination. With the assistance of polyvinylpyrrolidone and bromide ion, Pd nanocrystals with abundant catalytic sites were uniformly anchored on both the inner and surfaces of the Ni foam. Six chlorophenols were rapidly dechlorinated to phenol using Pd NCs/Ni with high conversion (> 98%) and selectivity (~ 100%). Pd NCs/Ni showed broad applicability to various reaction conditions and maintained stable activity over 12 consecutive cycles. The electrochemical hydrodechlorination follows the indirect dechlorination mechanism. Hydrogenolysis between adsorbed H and chlorophenols is the rate-controlling step. Low coordination Pd atoms on the faces of Pd (220) and Pd (311) are the main catalytic sites. The study provides a valuable insight of high performance and low cost Pd modified electrode and its catalytic mechanism in electrochemical hydrodechlorination.

1. Introduction

Chlorinated aromatic pollutants (CAPs) are widely found in natural aquatic environments, agricultural, industrial, pharmaceutical, and dye synthetic pesticide wastewater [1,2]. Most CAPs have strong carcinogenicity, biological toxicity, and environmental persistence due to the chlorine atoms in their molecular structures [3,4]. Therefore, several methods, including electrochemical oxidation, [5] chemical oxidation, [6] photocatalytic oxidation, [7] biodegradation, [8] zero-valent metal reduction, [9] catalytic reduction, [10] and electrochemical reduction [11] have been used to remove CAPs. Among these methods, electrochemical hydrodechlorination (HDC) can selectively remove chlorine from CAPs in polluted water under mild conditions. The dechlorinated products can be recycled and used as industrial raw materials or treated using subsequent low-cost biological processes. As a result, the electrochemical HDC has attracted considerable scholarly attention in environmental remediation.

Various metals, including Pd, [10–29] Pt, [30] Ru, [31] Co, [32] Ag, [33,34] Ni, [15,35] Pd-Au, [36] Cu-Fe, [37] and Fe-Ni, [38,39] have been used to catalyze the electrochemical HDC, among which Pd is considered the most active catalyst for the electrochemical HDC of CAPs. The electrochemical HDC of CAPs catalyzed using Pd can be described as follows:

$$Pd + 2\,H^+ \text{ (or } 2\,H_2O) + 2e^- \rightarrow Pd(2\,H)_{ads} \text{ (or } + 2OH^-) \quad (1)$$

$$Pd + RCl \leftrightarrow Pd(RCl)_{ads} \quad (2)$$

$$Pd(RCl)_{ads} + Pd(2\,H)_{ads} \rightarrow Pd(RH)_{ads} + Pd(HCl)_{ads} \quad (3)$$

$$Pd(HCl)_{ads} \leftrightarrow Pd + HCl \quad (4)$$

$$Pd(RH)_{ads} \leftrightarrow Pd + RH \quad (5)$$

Pd catalyst has excellent catalytic activity in electrochemical HDC owing to its ability to generate a strong reducing agent – the electrochemically adsorbed hydrogen (H_{ads}) from H^+ (or H_2O) at positive potentials (Eq. 1), and at the same time activate the C-Cl bond of RCl via its adsorption with CAPs (Eq. 2). Hydrogenolysis of CAPs then proceeds (Eq. 3) by reacting the adsorbed CAPs with H_{ads}, followed by desorption of the products (Eqs. 4 and 5).

However, Pd is a noble metal with few reserves, and it is expensive (the price of Pd was about 25 $/g in 2013 and rose nearly 3–4 times in

* Corresponding author.
E-mail address: xuyh@zjut.edu.cn (Y. Xu).

https://doi.org/10.1016/j.apcatb.2023.122978
Received 9 March 2023; Received in revised form 7 June 2023; Accepted 7 June 2023
Available online 9 June 2023

the last decade). Therefore, the development of a high-performance and low-loading Pd-modified electrode is crucial to catalyze electrochemical HDC. To achieve low-loading Pd-modified electrode with high HDC performance, scientists have mainly adopted the following two strategies: (1) improvement of the dispersion of Pd by increasing the specific surface area of the electrode substrate; [17,24,40,41] (2) enhancement the intrinsic activity of catalytic sites on Pd by strengthening the force between the substrate and the Pd (electronic effect). [16,25,27,28,42–44] Furthermore, some works also combine these two strategies to improve the performance of Pd modified electrodes. [13,18,26,38,45–48]. For example, Yang et al. deposited Pd particles on the Ni foam (3D structure). They found that the reaction rate constant of HDC using the Pd@Ni-foam electrode was 4.4 times higher than that of using Pd/C/Plate electrode [41]. Yu et al. coated Ni foam with an 3D network structure and electron-absorbing $NiCo_2O_4$ layer before depositing Pd, and the catalytic activity of Pd was increased by 6 times [26]. Although these efforts greatly improved the atomic utilization and activity of Pd, the low catalytic site density of Pd particles led to a high Pd consumption (usually 80 ~ 200 μg cm^{-2}) due to the uncontrolled Pd loading process. In addition, some efforts atomically dispersed Pd on catalysts, but these particles need to be recoated on carbon paper, which results in extremely uneven distribution of catalyst [15,49]. The high consumption of Pd significantly raised the cost of the treatment, thus limiting the application of the technology. Therefore, there is still a huge gap in the practical application requirements. However, numerous experiments have shown that Pd faces associated with a high density of low coordination atoms are generally more active for catalytic reactions [50]. Thus, we proposed a third strategy by increasing the density of catalytic sites (low coordination Pd atoms) and controlling the size and the morphology of Pd on the electrode.

In this study, a cuboctahedron Pd nanocrystal-modified Ni foam (Pd NCs/Ni) electrode with ultralow Pd loading (12.5 μg cm^{-2}) was first prepared via a polyvinyl pyrrolidone (PVP)- and bromide ion (Br^-)-assisted electrodeposition. Afterward, the activity of the Pd NCs/Ni electrode in electrochemical HDC was compared with the conventional Pd/Ni electrode at different current densities. Then, the operating conditions and reactants scopes of the Pd NCs/Ni electrode were investigated. Finally, the Pd mass activity (MA) of the Pd NCs/Ni electrode in HDC of 4-chlorophenol (4-CP) and 2,4-dichlorophenol (2,4-DCP) was compared with that of typical Pd-modified electrodes reported in the literature, and the dechlorination mechanism of 4-CP and the main catalytic site on Pd NCs/Ni were investigated. This study aimed to develop an easily prepared, high HDC performance, and ultra-low-loading Pd NCs/Ni electrode for dechlorinating CAPs in water. In addition, this study aimed to reveal the mechanism of the high catalytic activity of Pd NCs/Ni.

2. Experiments

2.1. Preparation of electrodes

Pd modified electrode was prepared by electrodeposition (Scheme 1). Concretely, Ni foam (20 mm × 20 mm × 2 mm, 110 PPI) was ultrasonicated in 20 mL acetone for 20 min to achieve complete de-oiling. Then, it was treated with 20 mL HNO_3 (0.5 mol L^{-1}) for 5 min to remove any oxides on the surface and washed with copious amounts of deionized water. The Pd NCs/Ni electrode was prepared via electrodeposition with an H-type cell divided by a Nafion-117 membrane (Fig. S1). Typically, 40 mL of 0.024 mmol L^{-1} Na_2PdCl_4 containing 0.1 mg of Pd^{2+} (optimal, Fig. S2) and 0.01 mol L^{-1} of HCl solution, 100 mg of PVP, and 400 mg of NaBr were added into the cathode chamber, and 40 mL of 0.1 mol L^{-1}, pH = 3, Phosphate Buffered Saline (PBS) was added into anode chamber. Before electrodeposition, the solution was stirred for 20 min to uniformly disperse the reagents. Then, the pre-treated Ni foam was used as a cathode and subjected to a current of 4 mA at 25 °C for 45 min until the color of the catholyte solution changed from light yellow to colorless. The Raman spectra indicates that residual PVP would not cover the electrode surface at the end of the electrodeposition, which should benefit from the reducing atmosphere of cathode (Fig. S3). The Pd/Ni electrode was prepared following the same process, but 568 mg of Na_2SO_4 was added to the electrode as the supporting electrolyte in place of adding PVP and NaBr. The ICP-MS (Inductively coupled plasma mass spectrometry, Table S1) results showed that more than 99% Pd ions in the solution were deposited onto the Ni foam, and the exact Pd loading was 12.5 μg cm^{-2}.

2.2. Electrochemical experiments

The electrochemical HDC experiments were performed in the H-type cell to prevent Cl_2 generation in anode (Fig. S1). Aliquots of samples were taken from the system after desired durations for further analysis. Precisely, 40 mL of PBS (0.1 mol L^{-1}, pH = 7) solutions containing 4-CP (1 mmol L^{-1}) was added into the cathode chamber. At the same time, 40 mL PBS (0.1 mol L^{-1}, pH = 7) was added into the anode chamber. The prepared electrode was used as the cathode, and a platinum plate was used as the anode. The electrochemical HDC were conducted under air and with a constant current of 6 mA for 180 min at 25 °C.

The Cyclic voltammetry (CV) was tested by CHI 660b workstation (Shanghai Chenhua), and a standard three-electrode system was used. Ag/AgCl (+0.2224 V vs. standard hydrogen electrode) filled with saturated potassium chloride solution was used as the reference electrode. Pt sheet was used as the counter electrode, and the prepared electrode was used as the working electrode. N_2 was pumped into the solution for 15 min to remove dissolved O_2. The electrochemically active surface area of electrodes was measured using CO-stripping analysis. Typically, at - 0.4 V, CO was pumped for 15 min to saturate the active sites of the electrode. Then, N_2 was bubbled for 15 min at open circuit to remove dissolved CO in the solution. Finally, the CV scan was conducted (from −0.4 to 0.8 V at a scan rate of 50 mV s^{-1}). Electrochemical impedance spectroscopy (EIS) test was conducted at - 0.6 V and a frequency range of 0.01–10000 Hz with an AC perturbation of 5 mV.

The MA of Pd was calculated under optimal conditions based on the quantity of reactants converted:

$$MA = \frac{M_{reactants} \times \alpha}{M_{Pd} \times t}$$

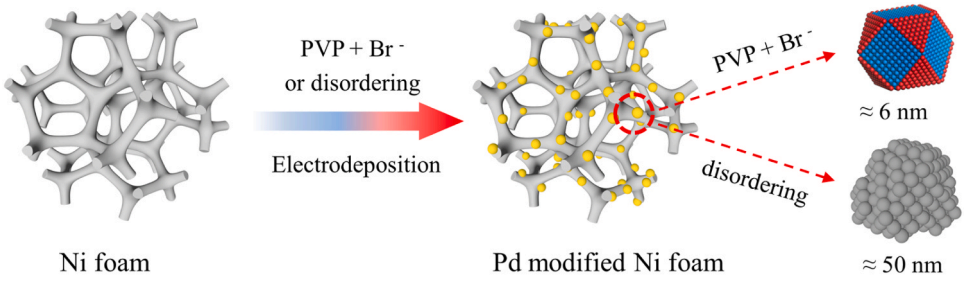

Scheme 1. The simple method to modify Pd on the Ni foam cathode.

where $M_{reactants}$ represents the moles of initial reactants (mmol), M_{pd} is the total Pd loading (g), α represents the conversion of reactants ($\alpha = 50\%$), and t is the electrolysis time (min).

A pseudo-first-order kinetic equation was used to describe the electrochemical HDC rate of 4-CP ($r_{4\text{-CP}}$), which is expressed as

$$r_{4-CP} = \frac{dC_{4-CP}}{dt} = -k \times C_{4-CP}$$

where $C_{4\text{-}CP}$ is the concentration of 4-CP (mol L^{-1}), t is the electrolysis time (h), and k is the reaction rate constant (h^{-1}). The k was calculated based on the amount of 4-CP converted (conversion of 4-CP < 50%).

The current efficiency (CE) was calculated as

$$CE = \frac{\Delta C_{4-CP} \times n \times F \times V}{\int_{t=0}^{t=t} Idt}$$

where $C_{4\text{-}CP}$ is the concentration of 4-CP (mol L^{-1}), n represents the number of electron transfers (n = 2 for 4-CP), t is the electrolysis time (s), F represents the Faraday constant (96485 C mol^{-1}), V is the catholyte volume (L), and I represents the electrolysis current (A).

2.3. Density functional theory (DFT) calculation

DFT calculation was performed using CP2K/Quickstep package [51]. A generalized gradient approximation of Perdew-Burke-Ernzerhof functional combined with DZVP-MOLOPT-SR-GTH basis set was adopted [52,53]. The DFT-D3 (BJ) model was used for weak interatomic interactions of dispersion correction, [54] and the input files were created using Multiwfn [55]. The Pd crystal was modeled using a p (4 × 4) supercell with at least five-layer slab thickness. The bottom two layers of atoms were fixed, while the top two layers of atoms and adsorbates were relaxed. The thickness of the vacuum layer between two adjacent plates was 15 Å. The parameters of the Monkhorst-Pack network for Brillouin zone integration were set to 2 × 2 × 1. The convergence threshold for ionic steps in geometry optimization was 5×10^{-6} eV. Geometries were deemed converged when the forces on each atom were below 4.5×10^{-4} eV/Å. The bridge site (Bri), face-centered cubic site (Fcc), hexagonal close-packed site (Hcp), and top site (Top) were chosen for the optimization of the adsorption structure of compounds (Tables S2–S5). Determine the optimal adsorption structure by comparing the lowest energy. The adsorption energies (E_{ads}) of

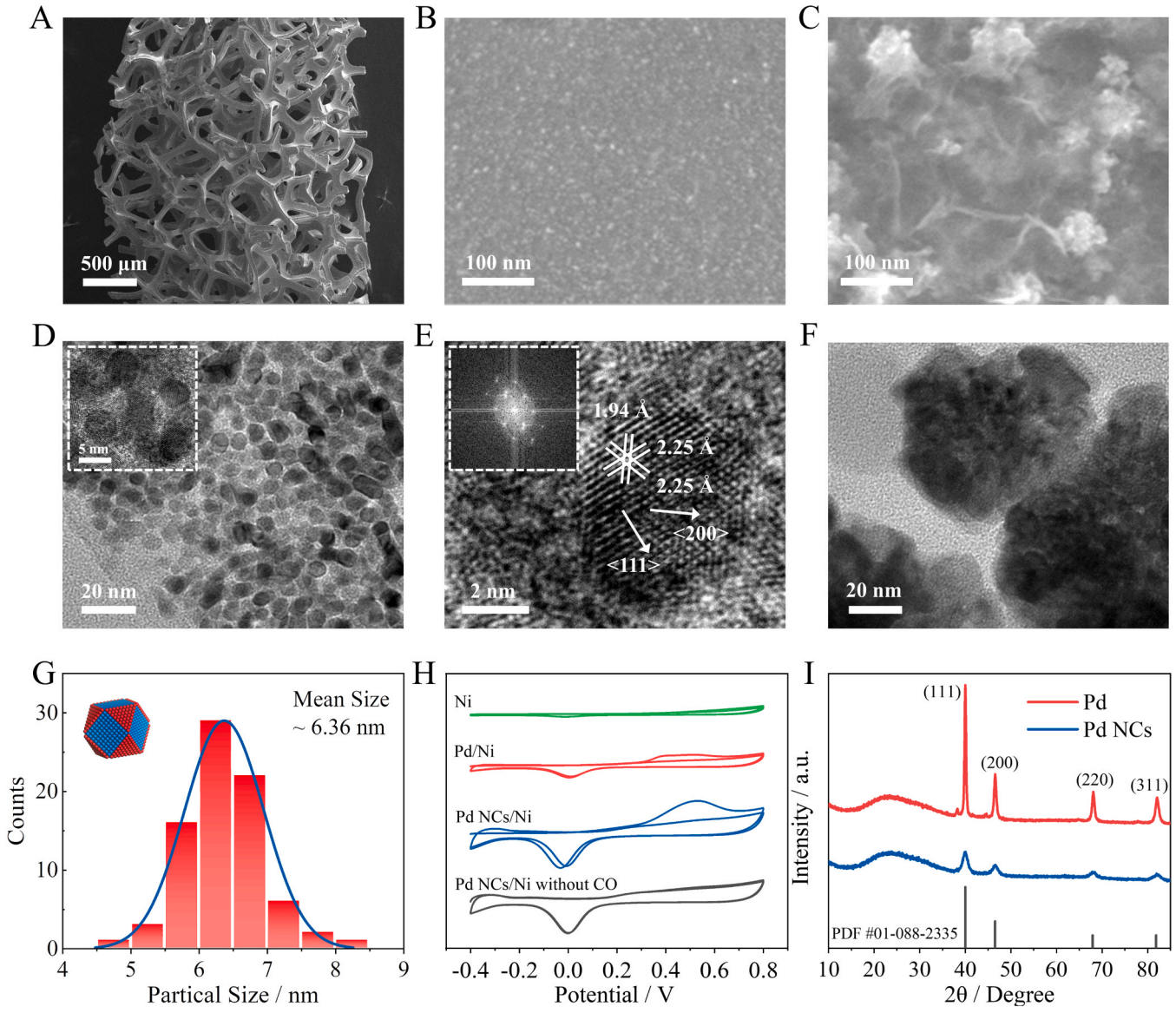

Fig. 1. SEM images of Pd NCs/Ni (A, B) and Pd/Ni (C); TEM images of Pd NCs (D, E) and Pd (F); (G) Size distributions of the Pd NCs; (H) Cyclic voltammetry curves of adsorbed CO stripping; (I) X-ray diffraction patterns of Pd NCs and Pd.

molecules were defined as $E_{ads} = E_{total} - E_{mol} - E_{sub}$, where E_{total}, E_{mol}, and E_{sub} are the total energies of the adsorbed system, the isolated molecule, and the clean substrate system, respectively.

3. Results and discussion

3.1. Characterization

Pd NCs/Ni exhibits the best performance for the electrochemical HDC of 4-CP, therefore its morphology was characterized in detail. Fig. 1A shows the scanning electron microscope image of the Pd NCs/Ni's cross-section. The porous structure of Ni foam provides a large area for Pd dispersion. Pd NCs are uniformly anchored on the Ni foam surface and exhibits fine sand-like morphology with a particle size of ~ 6.36 nm (Figs. 1B, D, and G). PVP endows Pd NCs with small size and high dispersion during electrodeposition. PVP can increases the steric hindrance around Pd and inhibit spontaneous agglomeration [56]. However, Pd particles on the conventional Pd/Ni tend to agglomerate and exhibit irregular cauliflower morphology (> 50 nm) because the electrodeposition is uncontrolled (Fig. 1C and F). The electrochemical active surface area of Pd NCs/Ni was measured using CO-stripping analysis (Fig. 1H), which is approximately 3.76 times than that of the Pd/Ni electrode. Furthermore, the distribution of Pd NCs in different regions of the Ni foam porous structure was observed to be relatively close (Fig. S4). This observation indicates that Pd NCs are uniformly distributed on the surface side of the electrode and uniformly distributed in the middle of the 3D framework of Ni foam. The increase in dispersion greatly improved the utilization of Pd atoms and significantly reduced their consumption.

TEM reveals that the Pd NCs have regular morphology and exhibit a single crystal structure of cuboctahedron, characterized by Pd (200) and Pd (111) faces (Fig. 1D and E). The Pd cuboctahedron is staggered by eight Pd (111) faces, six Pd (200) faces, twelve Pd (220) faces, and twenty-four Pd (311) faces [20]. Pd (220) and Pd (311) faces are formed on the edge of the Pd crystal, where Pd (220) is formed at the intersection of twain Pd (111) or of twain Pd (200), and Pd (311) is formed at the intersection of Pd (111) and Pd (200) (Fig. S5).

The coordination number of Pd (111), Pd (200), Pd (220), and Pd (311) faces are 9, 8, 7, and 7, respectively (Fig. S6). Pd (220) and Pd (311) faces are associated with the low coordination of Pd atoms. Pd belongs to Fcc clode packing, therefore it tends to form a structure with Pd (111) as the main exposed crystal face when the growth was not been intervened.

The results of X-ray diffraction (XRD) are shown in Fig. 1I, where the four diffraction peaks correspond to the typical Pd (111), Pd (200), Pd (220), and Pd (311) faces, respectively (PDF #01–088–2335). By measuring the relative strength of each peak with the main peak in XRD curve, the proportion of exposed faces can be quantified [57]. The relative intensities of XRD diffraction peaks including Pd (111), Pd (200), Pd (220), and Pd (311) of conventional Pd particles were measured to be 100%, 34%, 22%, and 19%, respectively. Whereas the intensities of Pd NCs turned to 100%, 47%, 30%, and 31%, respectively. These results shows that more Pd (200), Pd (220) and Pd (311) faces were exposed on Pd NCs.

The specific forming mechanism of Pd NCs could be described as the co-assisted of PVP and Br^-. As shown in Fig. S7, when PVP is only used as the assists in the electrodeposition, the size of Pd crystals decrease to ~ 6 nm, the shape of Pd crystals are diversified, and there are few low coordination Pd atoms (Fig. S8). The electrodeposition requires Br^- as another assist, which may be affected by the adsorption of Pd, especially Pd (200) face, on Br^- [58]. Although Br^- does not significantly reduce the particle size, it could increase the exposure of Pd (200) surface (Fig. S8). Finally, under the synergistic effect of PVP and Br^-, Pd NCs surfaces have more Pd (220) and Pd (311) exposure and abundant low coordination Pd atoms, which is contributed to the high density of the catalytic sites of Pd NCs/Ni [20,57].

3.2. Dechlorination performance of Pd NCs/Ni

3.2.1. Different electrodes

As shown in Fig. 2A, Pd NCs/Ni performs best electrochemical HDC activity: 4-CP (> 99.9%) was converted to phenol (PhOH) in an aqueous solution within 180 min (the selectivity of PhOH > 99.9%) on Pd NCs/Ni. The current of 6 mA is the optimal value for both Pd NCs/Ni and Pd/Ni catalyzed electrochemical HDC reaction (Table S6). For comparison, the amount of 4-CP removed on Pd/Ni under the same reaction condition is only 40% and with a low yield (33%) of phenol (Fig. 2B). Ni foam is mainly responsible for conducting electricity due to almost no electrochemical HDC activity to dechlorination (Fig. 2C). Time-potential curve proves that Pd NCs/Ni has higher catalytic activity due to its most positive cathode potential among these cathodes (Fig. S9). In addition, when PVP and Br^- individually takes part in the electrodeposition as the assists, the conversion of 4-CP is only 75% and 68%, respectively (Figure. S10), indicating that no matter reduce the particle size or control the crystal face, independently, there are limited effect on electrochemical HDC performance. NaCl has also been assessed as the nonideal assist in this electrodeposition system (Figure. S11). The results show that with the synergistic assistance of PVP and Br^-, Pd-modified electrode with better performance is expected to be obtained.

The reaction rate constant (k) corresponding to 4-CP electrochemical HDC was calculated using a pseudo-first-order kinetic formula. Although the same Pd loading of Pd NCs/Ni and Pd/Ni was used, the k of Pd NCs/Ni is ~ 8 times larger than that of Pd/Ni (Figs. 2A and 2B). This result confirms that Pd NCs/Ni has much higher intrinsic activity than the conventional Pd /Ni, since the electrochemically active area of Pd on Pd NCs/Ni is 3.76 times that of Pd/Ni. The high activity of Pd NCs/Ni is attributed to (i) the apparent activity of uniform dispersion and small Pd size (large electrochemical active area) and (ii) the intrinsic activity of abundant low coordination Pd atoms on surface (high density of catalytic sites).

By comparing the CE of 4-CP electrochemical HDC carried on each electrode (Fig. 2D), Pd NCs/Ni has a considerable efficiency advantage. This indicates that 4-CP hydrogenates faster on Pd NCs/Ni, slower on Pd/Ni and inert on Ni. The CE of Pd NCs/Ni increased from 15 to 30 min, then decreased over time. The changing trend of CE is related to the concentration of the reactant and the H_{ads}. Despite the high concentration of 4-CP at the beginning, the dissolved oxygen in aqueous solution and the hydrogen storage of Pd [21] could limited the rate of electrochemical HDC. With the reduction of oxygen and the filling of storage hydrogen, there are more H_{ads} on the surface. As a result, CE increases gradually. After 30 min, as the concentration of 4-CP gradually decreases, H_{ads} is abundant and converted into H_2 follows decreased CE.

3.2.2. Various conditions

Considering the practical applications, Pd NCs/Ni must be able to withstand different concentrations and supporting electrolytes. As shown in Table 1, under the concentration range of 0.01–1 mmol L^{-1}, 4-CP could be fully degraded (Table 1, entries 1–3). There are almost no negative effect on the electrochemical HDC of the changing supporting electrolyte (Na_2SO_4 and NaCl) and concentration (2 or 50 mmol L^{-1}), where 4-CP could be eliminated (Table 1, entries 8–10). Pd NCs/Ni is immunity to various reaction conditions indicating that Pd NCs/Ni can effectively treat polluted wastewater at certain reaction conditions.

Unless otherwise noted, Pd NCs/Ni was served as the cathode (reaction time = 3 h, current = 6 mA, T = 25 ℃ and pH = 7). [a] The applied current was set at 4 mA; [b] The pH of catholyte solution was set at 3. [c] The temperature was set at 40 ℃. (mM = mmol L^{-1}).

3.2.3. Reactant scope and stability

Chlorophenols, including 2-chlorophenol (2-CP), 3-chlorophenol (3-CP), 4-CP, 2,4-dichlorophenol (2,4-DCP), 2,5-dichlorophenol (2,5-DCP), 3,5-dichlorophenol (3,5-DCP), 2,6-dichlorophenol (2,6-DCP), and 2,4,6-trichlorophenol (2,4,6-TCP), are a series of typical CAPs pollutants, and

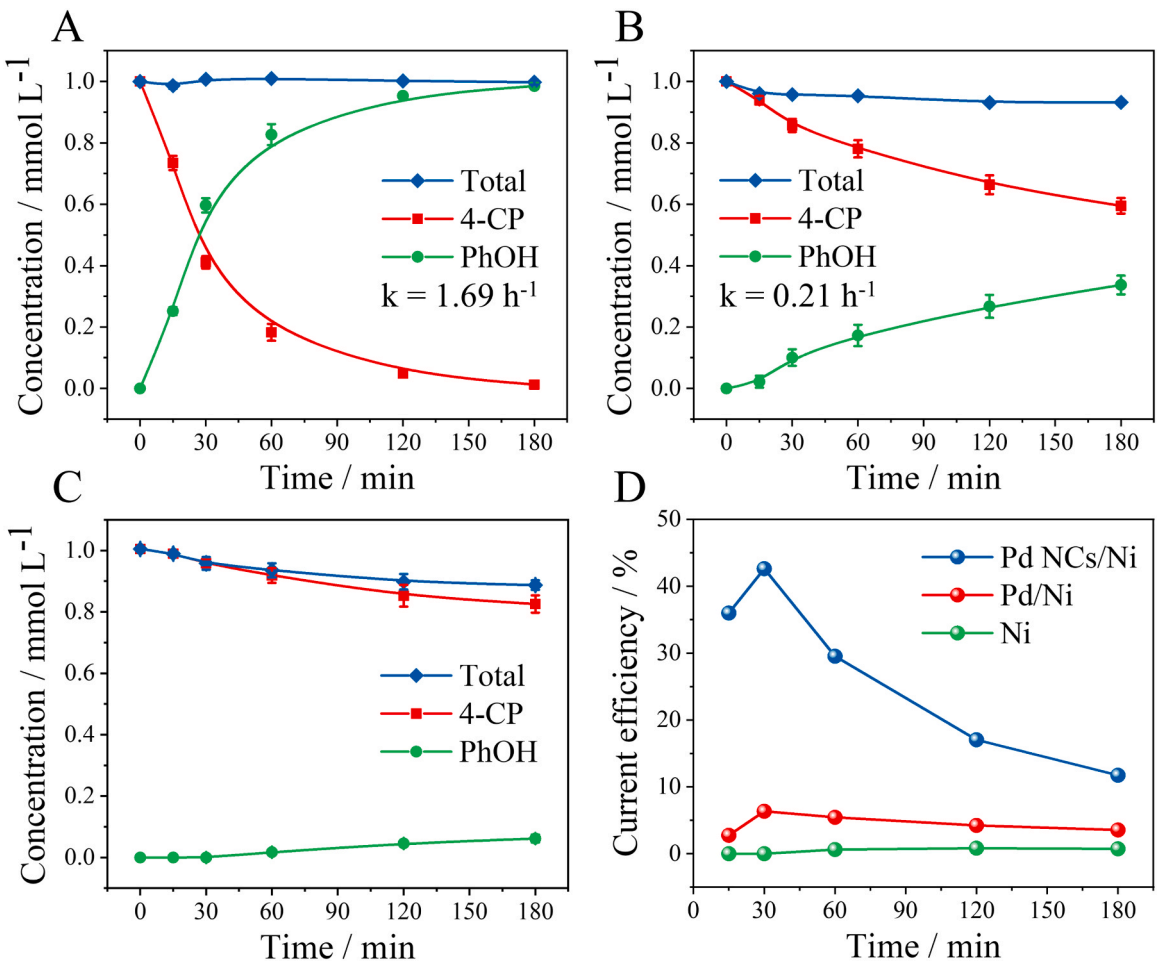

Fig. 2. Dechlorination performance of Pd NCs/Ni (A), Pd/Ni (B), and Ni (C); (D) Current efficiency corresponding to A, B and C; k is the reaction rate constant.

Table 1
Simulation of various reaction conditions.

Entry	$C_{4\text{-}CP}$/mM	electrolyte	Removal rat%
1	1	100 mM PBS	99.9
2[a]	0.1	100 mM PBS	99.9
3[a]	0.01	100 mM PBS	99.9
4	1	50 mM Na_2SO_4[c]	95.2
5	1	50 mM NaCl[c]	94.0
6	1	50 mM Na_2SO_4[b]	99.9
7[a]	0.1	2 mM Na_2SO_4	94.7
8[a]	0.1	2 mM Na_2SO_4[c]	99.9
9[a]	0.1	2 mM Na_2SO_4[b]	99.9
10[a]	0.1	2 mM NaCl[c]	99.9

these CAPs can be found in agricultural, industrial, and pharmaceutical wastewaters. The electrochemical HDC electrolysis of these CAPs was carried out using Pd NCs/Ni. As shown in Figs. 3A–3 F, 4-CP, 2-CP, 3-CP, 2,4-DCP, 2,5-DCP, and 3,5-DCP were rapidly dechlorinated with high conversion (> 98%) and high selectivity (PhOH, ~ 100%). In addition, the conversion of 2,6-DCP and 2,4,6-TCP were more than 92%, although the selectivity of PhOH was ~81 and ~ 53%, respectively, the by-products were low toxic and with less chlorine (Fig. 3 G and 3 H). The different efficiencies of electrochemical HDC may be related to the different values of pK_a (acidity coefficient) of various chlorophenols. In an aqueous solution, the pK_a order of the above chlorophenols is as follows: 4-CP > 3-CP > 2-CP > 3,5-DCP > 2,4-DCP > 2,5-DCP > 2,6-DCP > 2,4,6-TCP. According to the Henderson–Hasselbach balance equation, chlorophenols have different degrees of protonation in the same aqueous solution (Table S7). The electron repulsion between chlorophenolates and electrode inhibited adsorption as the cathode was negatively charged [19]. The strength of the repulsion is inversely proportional to the value of the pKa, even though the majority of various chlorophenols were fully hydrogenated on Pd NCs/Ni.

High-performing electrode materials maintaining stability in multiple cycles is crucial. As shown in Fig. 3I, Pd NCs/Ni maintained good efficiency in 12 cycles electrolysis of 4-CP. Through the ICP-MS test, we have found that the Pd loss on Pd NCs/Ni after the electrolysis is about 0.038 wt% suggesting that Pd NCs have good stability (Table S8). However, the performance of Pd/Ni rapidly declined because the cauliflower Pd on the surface is loosely bound (Fig. S12 and Table S8). The stability of Pd NCs/Ni electrodes could be attributed to the fine distribution of Pd NCs and their strong in-situ anchoring on the substrate. In contrast, coating Pd catalyst to carbon paper via Nafion gluing, the ex-situ Pd modified cathode appears to be very less stable, as the catalyst is easily shed [15,24].

3.2.4. *Catalytic activity comparison*

The MA of the Pd-modified cathode is the main technical index of electrochemical HDC methods. MA determined the amount of Pd used in the treatment per unit of CAPs in unit time. We compared the MA of Pd NCs/Ni with other Pd-modified electrodes in the literature. As shown in Fig. 4, Pd NCs/Ni exhibits the highest MA value in the electrochemical HDC of both 4-CP and 2,4-DCP in various cathodes. This result demonstrates that the Pd atoms utilization of Pd NCs/Ni is topmost compared to other cathodes. At the same time, Pd NCs/Ni has the lowest Pd loading compared to literature reports. In addition, we have

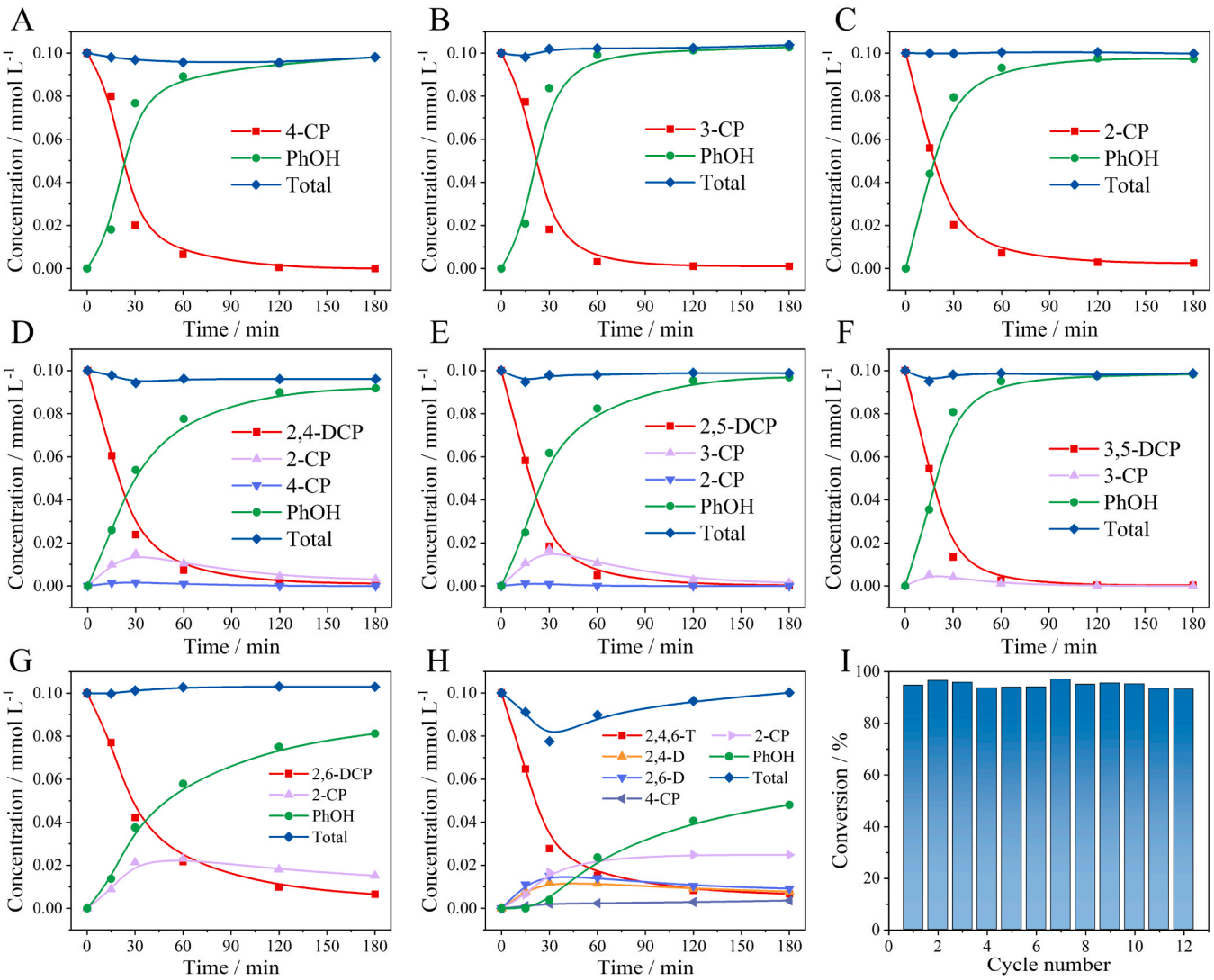

Fig. 3. (A - H) EHDC performance of Pd NCs/Ni towards various chlorophenols. Unless otherwise noted, all reaction conditions were kept the same as those in Entry 9 of Table 1; (I) Cyclic stability of Pd NCs/Ni to 4-CP, the reaction time of each cycle was 60 min; The electrolytic current of D, E, F, G and H was 6 mA.

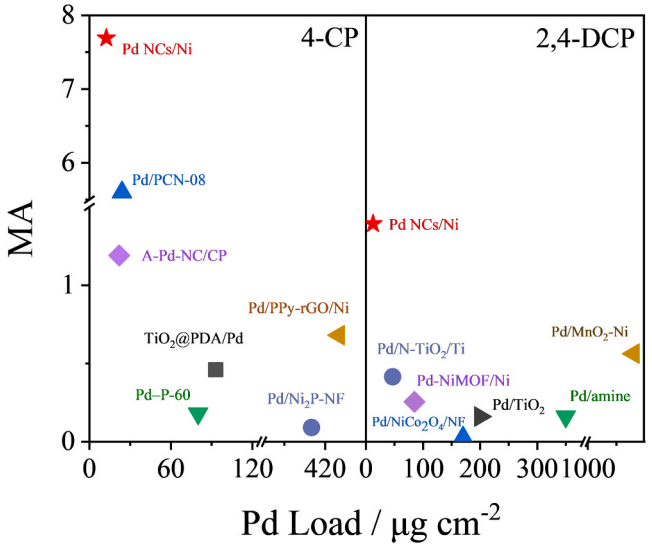

Fig. 4. MA Comparison of various Pd modified cathodes in electrochemical HDC of 4-CP and 2,4-DCP.

calculated the ratio of pseudo-first-order kinetic constant (k, min^{-1}) and the catalyst concentration (C_o, g L^{-1}). As can be seen from Table S9, the k/C_o of Pd NCs/Ni is still far exceeds that of other Pd-modified electrodes. Therefore, the high MA and k/C_o suggest that Pd NCs/Ni is relatively competitive in the application.

3.3. Mechanism

3.3.1. Catalytic mechanism and rate-controlling step

To reveal the catalytic mechanism of the Pd NCs/Ni on 4-CP electrochemical HDC, CV tests were first perfomed to confim the reaction process. As shown in Fig. 5A, the CV scan was first performed on a 0.1 mol L^{-1} PBS aqueous solution (Blank solution) within the potential range of 0 ~ - 0.6 V. There are two distinct pairs of reversible redox peaks (A_1 and A_2, B_1 and B_2). According to these characteristic peaks, A_1 and A_2 correspond the reduction of H_2O/H^+ to H_{ads} and the re-oxidization of H_{ads}, respectively. B_1 and B_2 are attributed to the absorbed hydrogen atom (H_{abs}) and the re-oxidization of H_{abs}, respectively [15,22]. In addition, at - 0.8 V, the response current rapidly rose, representing H_2 evolution (Fig. 5C). As a result, the classical steps of water splitting are occurred on Pd NCs/Ni at negative potential. As shown in Fig. 5B, when 4-CP was added to the blank solution, the current response of A_1 sharply rose and A_2 decreased. Meanwhile, no new reduction

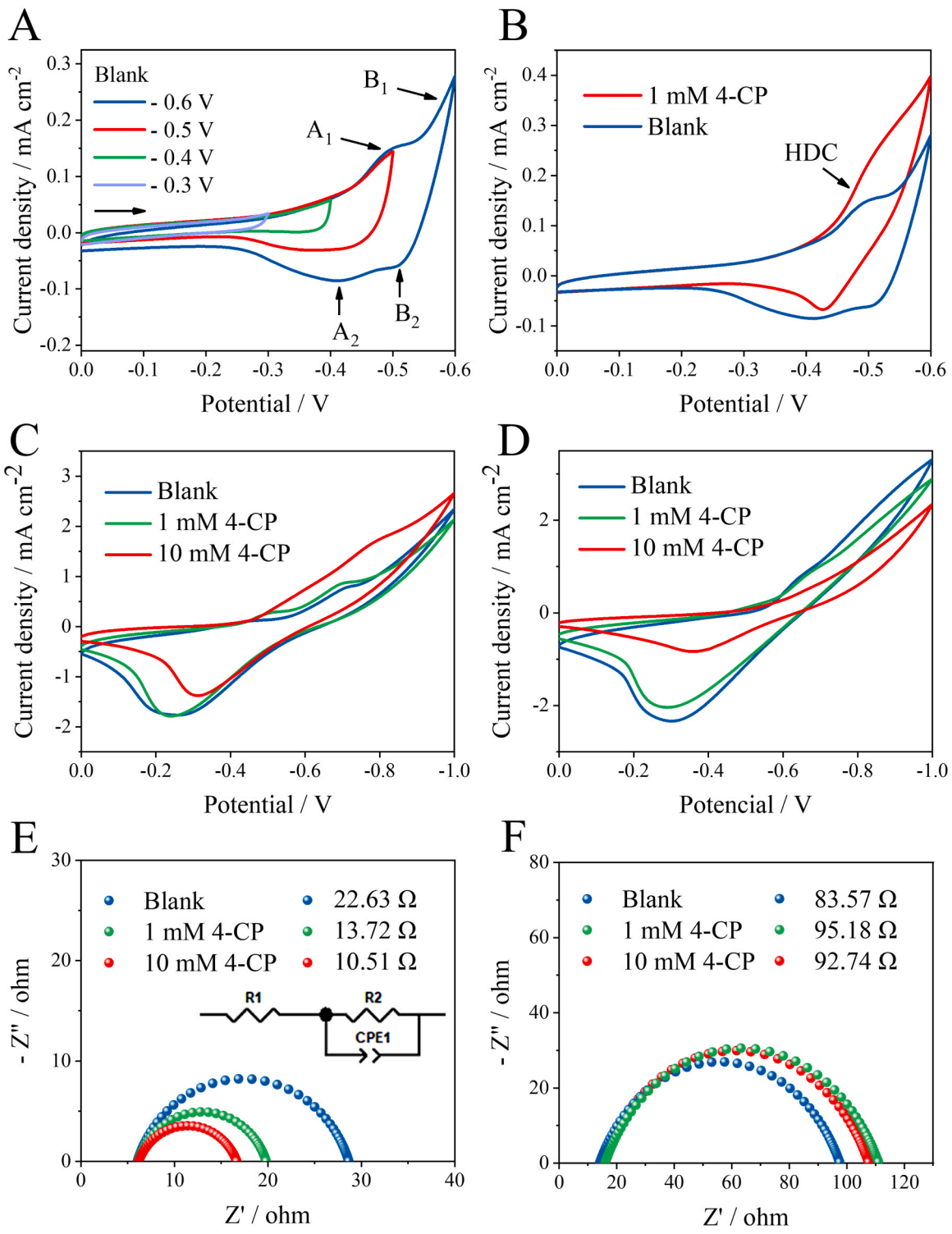

Fig. 5. Cyclic voltammograms of Pd NCs/Ni (A, B and C) and Pd/Ni (D). Nyquist plots of Pd NCs/Ni (E) and Pd/Ni (F). Blank solution: a N_2-saturated 0.1 M phosphate buffer saline at pH = 7.

current responses appearing. This observation indicates that the electrochemical HDC is consistent with the indirect hydrodechlorination mechanism with H_{ads} as the reductant. This conclusion could be further supported by Fig. S13, with the increasing concentrations of 4-CP, the reduction current response becoming stronger, and the corresponding oxidation peak turning smaller.

It is worth noting that the CV current response of Pd NCs/Ni is rapidly zooming under the influence of 4-CP of high concentration (Fig. 5C). The increasing CV current response is accompanied by a rapid mass transfer and charge transfer. The quickly reaction of 4-CP with H_{ads} on Pd NCs/Ni enlarges the concentration gradient of 4-CP between the electrode surface and the bulk solution and resulted in a rapid rise of current in CV. However, the reduction current of Pd/Ni decreased when 4-CP could not rapidly react with H_{ads} in time. The excessive 4-CP on the electrode surface and H_{ads} will form a competitive relationship, resulting in a drop in current (Fig. 5D). These results indicate that Pd NCs/Ni

exhibited exceptionally high catalytic activity against 4-CP, while Pd/Ni has weak activity.

The kinetic properties of electrochemical HDC catalyzed by different electrodes were further measured by EIS. The fitting of charge transfer impedance (R_{ct}) in the high-frequency region of Pd NCs/Ni and Pd/Ni are presented in Figs. 5E and 5F, respectively. The equivalent circuit fitting is shown in the inset of Fig. 5E. Diameter of the semicircle presented the R_e between charges of the electrode and reactants of electrolyte [46]. In the blank solution and at an applied potential of − 0.6 V, the R_{ct} values of Pd NCs/Ni and Pd/Ni were 22.63 and 83.57 Ω, respectively. The contribution of Ni at the above potential can be ignored owing to the impedance higher than 800 Ω (Figure. S14). The R_{ct} of Pd/Ni is 3.69 times than that of Pd NCs/Ni, similar to the multiples of their electrochemically active area (1/3.76 times), which is consistent with the law of resistance. Therefore, Pd NCs/Ni and Pd/Ni have the same ability to catalyze and reduce H_2O (or H^+) to H_{ads} (H_{ads} generating reaction). In addition, the obtained CE are relatively low (Fig. 2D) as the excessive H_{ads} were evolutes to H_2. It suggests that the H_{ads} generating reaction is not the rate-controlling step for electrochemical HDC [59, 60].

After the 4-CP of different concentrations was added to the blank solution, the R_{ct} of Pd NCs/Ni rapidly decreased (Fig. 5E) in contrast to Pd/Ni (Fig. 5F) as the addition of 4-CP accelerated electron transfer on the Pd NCs/Ni surface. It confirmed that the high catalytic activity of Pd NCs/Ni is mainly attributed to the accelerated charge transfer in the hydrogenolysis step ($Pd(RCl)_{ads} + Pd(2\ H)_{ads} \rightarrow Pd(RH)_{ads} + Pd(HCl)_{ads}$).

Consequently, the hydrogenolysis step is the rate-controlling step of the electrochemical HDC, and it can facilitate electrochemical HDC. Pd NCs/Ni has higher intrinsic activity to accelerate the hydrogenolysis step. It is precisely the inside reason for Pd NCs/Ni to have such a high electrochemical HDC property.

3.3.2. DFT calculation

To further study the accelerating mechanism of Pd NCs toward hydrogenolysis, the adsorption energies (E_{ads}) of Pd (200), Pd (220), Pd (111), and Pd (311) to 4-CP and PhOH were calculated using DFT (Fig. 6). First, the E_{ads} of 4-CP and PhOH on the Pd (200) are − 2.90 and − 2.91 eV, respectively. At the same time, the E_{ads} of 4-CP and PhOH on Pd (111) are − 2.36 and − 2.37 eV, respectively. The E_{ads} of PhOH on Pd (200) and Pd (111) exceeds that of 4-CP. It indicates PhOH could not be easily desorbed but competed with 4-CP by adsorbing on Pd (200) and Pd (111) faces. In addition, the E_{ads} of HCl on Pd was calculated, which is much lower than that of 4-CP and PhOH (Table S10). This phenomenon indicates that another product (HCl) of the hydrogenolysis reaction is liable to desorption and will not hinder the reaction.

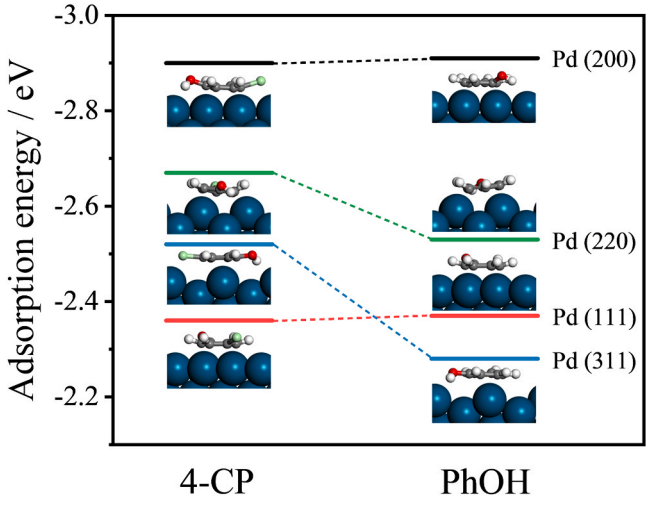

Fig. 6. The adsorption energies of 4-CP and PhOH on Pd (200), Pd (220), Pd (111) and Pd (311) facets under the optimized configuration.

The competitive adsorption of PhOH as a product will block the catalytic sites and then inhibit the hydrogenolysis reaction ($Pd(RCl)_{ads} + Pd(2\ H)_{ads} \rightarrow Pd(RH)_{ads} + Pd(HCl)_{ads}$). [59] Therefore, the Pd atoms on Pd (200) and Pd (111) are not the main catalytic sites of hydrogenolysis. However, the E_{ads} of PhOH on Pd (220) is − 2.53 eV, which is − 0.14 eV lower than that of 4-CP (−2.67 eV). The E_{ads} of PhOH on Pd (311) was − 2.28 eV, which decreased by 0.24 eV compared with 4-CP (−2.52 eV). This result shows that PhOH desorbed from Pd (220) and Pd (311) are more spontaneous, where the reactive sites would not be congested.

Therefore, low coordination Pd atoms on the Pd (220) and Pd (311) of Pd NCs are the main catalytic sites of electrochemical HDC, which is attributed to the high intrinsic activity (Scheme 2). The indirect dechlorination path of CAPs catalyzed by Pd NCs/Ni is illustrated in Scheme 2A. H_{ads} are generated at cathode and at the same time the C-Cl bond of RCl is actived via its adsorption by Pd. Hydrogenolysis then proceeds, followed by desorption of the products. Low coordination Pd atoms displays essential roles during this process, which could make the product quickly desorption, thereby swiftly refresh the reaction site in time, and facilitating the reaction continuous. The calculation of DFT matches well with the experimental results. The excellent electrochemical HDC performance of Pd NCs/Ni is attributed to the high dispersion, the small size of Pd NCs, and the unique crystal structure.

4. Conclusions

In summary, the Pd nanocrystals (Pd NCs) with a high density of catalytic sites were loaded on Ni foam via the Br^- and PVP-assisted electrodeposition method. Pd NCs/Ni exhibited the highest MA compared with various Pd-modified electrodes in the latest reports. The reaction rate constant of Pd NCs/Ni (1.69 h^{-1}) was 8 times higher than that of Pd/Ni (0.21 h^{-1}). Six chlorophenols were rapidly dechlorinated to phenol with high conversion (> 98%) and selectivity (~100%). Pd NCs/Ni exhibited a stable property over 12 cycles of electrolysis and immunity to various reaction conditions. The dechlorination reaction followed the indirect hydrodechlorination mechanism with electrochemically adsorbed hydrogen (H_{ads}) as the reductant. The hydrogenolysis between H_{ads} and chlorophenols was the rate-controlling step. Low coordination Pd atoms on the Pd (220) and Pd (311) faces were the main catalytic sites, which accelerated the hydrogenolysis, thereby significantly improving the intrinsic activity of Pd NCs/Ni in electrochemical HDC. This work provides valuable insights into the study of low-loading Pd-modified electrodes, the catalytic mechanism of electrochemical HDC, and the application prospect for Pd-catalyzed electrochemical HDC.

CRediT authorship contribution statement

Huan Wu: Investigation, Methodology, Visualization, Writing - original draft. **Zhechuan Mao:** Investigation, Software. **Baoquan Liu:** Validation, Visualization. **Deyin Chen:** Investigation. **Meiqin Shi:** Formal analysis, Resources. **Bosheng Lv:** Resources. **Yinghua Xu:** Resources, Conceptualization, Funding acquisition, Project administration, Writing - review & editing. **Lianbang Wang:** Resources.

Declaration of Competing Interest

We declare that we have no financial and personal relationships with other people or organizations that can inappropriately influence our work, there is no professional or other personal interest of any nature or kind in any product, service and/or company that could be construed as influencing the position presented in, or the review of, the manuscript entitled.

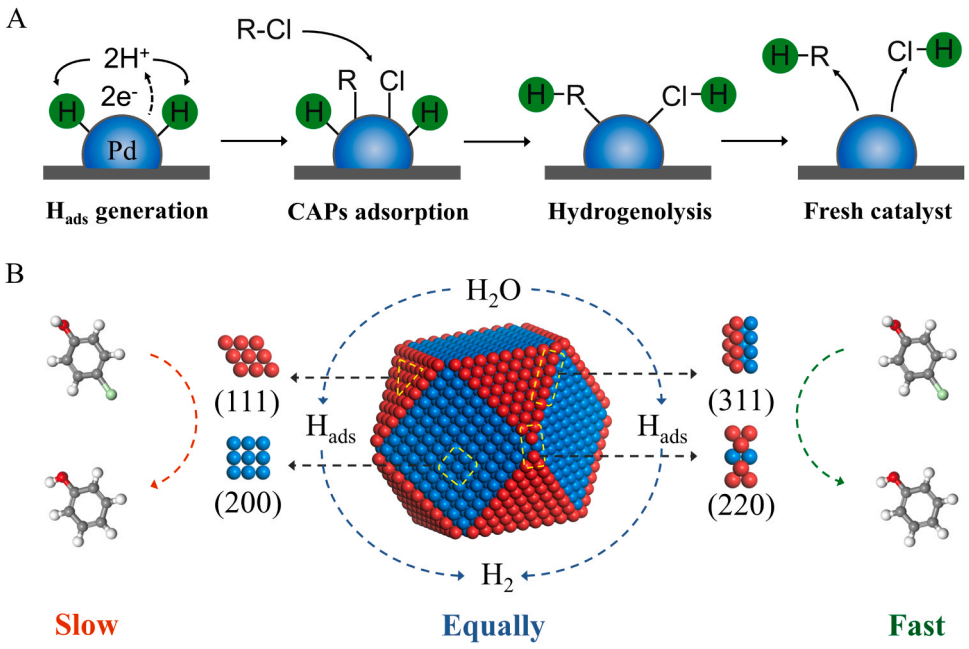

Scheme 2. (A) Indirect dechlorination path of CAPs catalyzed by Pd NCs/Ni; (B) Catalytic sites of electrochemical HDC on the surface of Pd NCs.

Data Availability

Data will be made available on request.

Acknowledgement

This work was supported by the funds from the National Natural Science Foundation of China (21576238, 21106133), the Natural Science Foundation of Zhejiang Province, China (LY16B060012), Zhejiang Provincial Key Research and Development Program (2020C03085), and Public Welfare Research Program of Zhejiang Province, China (LGF20B070004).

Appendix A. Supporting information

Supplementary data associated with this article can be found in the online version at doi:10.1016/j.apcatb.2023.122978.

References

[1] G. Xu, X. Zhao, S. Zhao, C. Chen, M.J. Rogers, R. Ramaswamy, J. He, Insights into the occurrence, fate, and impacts of halogenated flame retardants in municipal wastewater treatment plants, Environ. Sci. Technol. 55 (2021) 4205–4226, https://doi.org/10.1021/acs.est.0c05681.

[2] D.N. Bulloch, E.D. Nelson, S.A. Carr, C.R. Wissman, J.L. Armstrong, D. Schlenk, C. K. Larive, Occurrence of halogenated transformation products of selected pharmaceuticals and personal care products in secondary and tertiary treated wastewaters from Southern California, Environ. Sci. Technol. 49 (2015) 2044–2051, https://doi.org/10.1021/es504565n.

[3] D. Rosner, G. Markowitz, Persistent pollutants: a brief history of the discovery of the widespread toxicity of chlorinated hydrocarbons, Environ. Res. 120 (2013) 126–133, https://doi.org/10.1016/j.envres.2012.08.011.

[4] B. McHugh, R. Poole, J. Corcoran, P. Anninou, B. Boyle, E. Joyce, M. Barry Foley, E. McGovern, The occurrence of persistent chlorinated and brominated organic contaminants in the European eel (Anguilla anguilla) in Irish waters, Chemosphere 79 (2010) 305–313, https://doi.org/10.1016/j.chemosphere.2010.01.029.

[5] Y.-Y. Lou, F. Geneste, I. Soutrel, A. Amrane, F. Fourcade, Alachlor dechlorination prior to an electro-Fenton process: Influence on the biodegradability of the treated solution, Sep. Purif. Technol. 232 (2020), https://doi.org/10.1016/j.seppur.2019.115936.

[6] C.E. Schaefer, P. Ho, E. Berns, C. Werth, Mechanisms for abiotic dechlorination of trichloroethene by ferrous minerals under oxic and anoxic conditions in natural sediments, Environ. Sci. Technol. 52 (2018) 13747–13755, https://doi.org/10.1021/acs.est.8b04108.

[7] W. Guo, Y. Qin, C. Liu, B. Guo, J. Zou, Z. Xie, L. Wu, Unveiling the intermediates/pathways towards photocatalytic dechlorination of 3,3′,4,4′-trtrachlorobiphenyl over Pd /TiO2(B) nanosheets, Appl. Catal. B: Environ. 298 (2021), https://doi.org/10.1016/j.apcatb.2021.120526.

[8] T.P. Needham, R.B. Payne, K.R. Sowers, U. Ghosh, Kinetics of PCB microbial dechlorination explained by freely dissolved concentration in sediment microcosms, Environ. Sci. Technol. 53 (2019) 7432–7441, https://doi.org/10.1021/acs.est.9b01088.

[9] J. Blotevogel, R.J. Giraud, T. Borch, Reductive defluorination of perfluorooctanoic acid by zero-valent iron and zinc: a DFT-based kinetic model, Chem. Eng. J. 335 (2018) 248–254, https://doi.org/10.1016/j.cej.2017.10.131.

[10] J. Li, M. Li, J. Li, S. Wang, G. Li, X. Liu, Hydrodechlorination and deep hydrogenation on single-palladium-atom-based heterogeneous catalysts, Appl. Catal. B: Environ. 282 (2021), https://doi.org/10.1016/j.apcatb.2020.119518.

[11] R. Liu, H. Zhao, X. Zhao, Z. He, Y. Lai, W. Shan, D. Bekana, G. Li, J. Liu, Defect sites in ultrathin Pd nanowires facilitate the highly efficient electrochemical hydrodechlorination of pollutants by H*ads, Environ. Sci. Technol. 52 (2018) 9992–10002, https://doi.org/10.1021/acs.est.8b02740.

[12] M.A. Álvarez-Montero, L.M. Gómez-Sainero, M. Martín-Martínez, F. Heras, J. J. Rodriguez, Hydrodechlorination of chloromethanes with Pd on activated carbon catalysts for the treatment of residual gas streams, Appl. Catal. B: Environ. 96 (2010) 148–156, https://doi.org/10.1016/j.apcatb.2010.02.012.

[13] J. Li, Y. Chen, R. Bai, C. Chen, W. Wang, Y. Pan, Y. Liu, Construction of Pd/Ni2P-Ni foam nanosheet array electrode by in-situ phosphatization-electrodeposition strategy for synergistic electrocatalytic hydrodechlorination, Chem. Eng. J. 435 (2022), 134932, https://doi.org/10.1016/j.cej.2022.134932.

[14] Y.Y. Lou, C. Xiao, J. Fang, T. Sheng, L. Ji, Q. Zheng, B.B. Xu, N. Tian, S.G. Sun, High activity of step sites on Pd nanocatalysts in electrocatalytic dechlorination, Phys. Chem. Chem. Phys. 24 (2022) 3896–3904, https://doi.org/10.1039/d1cp04975e.

[15] Z. Mao, L. Liu, H.B. Yang, Y. Zhang, Z. Yao, H. Wu, Y. Huang, Y. Xu, B. Liu, Atomically dispersed Pd electrocatalyst for efficient aqueous phase dechlorination reaction, Electrochim. Acta 391 (2021), 138886, https://doi.org/10.1016/j.electacta.2021.138886.

[16] Y. Chen, Z. Liu, S. Liu, Y. Cheng, C. Zhang, J. Jiao, Y. Lu, W. Wang, K. Sun, X. Bi, A. Han, B. Liu, Y. Pan, Y. Liu, C. Liu, In-Situ doping-induced crystal form transition of amorphous Pd–P catalyst for robust electrocatalytic hydrodechlorination, Appl. Catal. B: Environ. 284 (2021), 119713, https://doi.org/10.1016/j.apcatb.2020.119713.

[17] Y. Shen, Y. Tong, J. Xu, S. Wang, J. Wang, T. Zeng, Z. He, W. Yang, S. Song, Ni-based layered metal-organic frameworks with palladium for electrochemical dechlorination, Appl. Catal. B: Environ. 264 (2020), 118505, https://doi.org/10.1016/j.apcatb.2019.118505.

[18] Z. Lou, J. Zhou, M. Sun, J. Xu, K. Yang, D. Lv, Y. Zhao, X. Xu, MnO2 enhances electrocatalytic hydrodechlorination by Pd/Ni foam electrodes and reduces Pd needs, Chem. Eng. J. 352 (2018) 549–557, https://doi.org/10.1016/j.cej.2018.07.057.

[19] G. Jiang, K. Wang, J. Li, W. Fu, Z. Zhang, G. Johnson, X. Lv, Y. Zhang, S. Zhang, F. Dong, Electrocatalytic hydrodechlorination of 2,4-dichlorophenol over palladium nanoparticles and its pH-mediated tug-of-war with hydrogen evolution, Chem. Eng. J. 348 (2018) 26–34, https://doi.org/10.1016/j.cej.2018.04.173.

[20] X. Ding, Z. Yao, Y. Xu, B. Liu, Q. Liu, Y. She, Aqueous-phase hydrodechlorination of 4-chlorophenol on palladium nanocrystals: Identifying the catalytic sites and unraveling the reaction mechanism, J. Catal. 368 (2018) 336–344, https://doi.org/10.1016/j.jcat.2018.10.008.

[21] G. Jiang, M. Lan, Z. Zhang, X. Lv, Z. Lou, X. Xu, F. Dong, S. Zhang, Identification of active hydrogen species on palladium nanoparticles for an enhanced electrocatalytic hydrodechlorination of 2,4-dichlorophenol in water, Environ. Sci. Technol. 51 (2017) 7599–7605, https://doi.org/10.1021/acs.est.7b01128.
[22] H. Ma, Y. Xu, X. Ding, Q. Liu, C.-A. Ma, Electrocatalytic dechlorination of chloropicolinic acid mixtures by using palladium-modified metal cathodes in aqueous solutions, Electrochim. Acta 210 (2016) 762–772, https://doi.org/10.1016/j.electacta.2016.06.001.
[23] J. Lyu, J. Wang, C. Lu, L. Ma, Q. Zhang, X. He, X. Li, Size-dependent halogenated nitrobenzene hydrogenation selectivity of Pd nanoparticles, J. Phys. Chem. C. 118 (2014) 2594–2601, https://doi.org/10.1021/jp411442f.
[24] Q. Wang, L. Zhou, Q. Chen, M. Mao, W. Jiang, Y. Long, G. Fan, Oxygenated functional group-driven spontaneous fabrication of Pd nanoparticles decorated porous carbon nanosheets for electrocatalytic hydrodechlorination of 4-chlorophenol, J. Hazard. Mater. 408 (2021), 124456, https://doi.org/10.1016/j.jhazmat.2020.124456.
[25] X. Wei, J. Wang, J. Miao, R. Zhang, W. Lu, N. Zhang, X. Zhou, H. Xu, J. Zhang, S. Peng, Enhanced performance of an in-situ synthesized Pd/N-TiO2/Ti cathode for electrocatalytic hydrodechlorination, Colloids Surf. A Physicochem. Eng. Asp. 648 (2022), 129320, https://doi.org/10.1016/j.colsurfa.2022.129320.
[26] W. Yu, H. Jiang, J. Fang, S. Song, Designing an electron-deficient Pd/NiCo2O4 bifunctional electrocatalyst with an enhanced hydrodechlorination activity to reduce the consumption of Pd, Environ. Sci. Technol. 55 (2021) 10087–10096, https://doi.org/10.1021/acs.est.1c01922.
[27] G. Jiang, X. Shi, M. Cui, W. Wang, P. Wang, G. Johnson, Y. Nie, X. Lv, X. Zhang, F. Dong, S. Zhang, Surface ligand environment boosts the electrocatalytic hydrodechlorination reaction on palladium nanoparticles, ACS Appl. Mater. Interfaces 13 (2021) 4072–4083, https://doi.org/10.1021/acsami.0c20994.
[28] J. Li, Y. Peng, W. Zhang, X. Shi, M. Chen, P. Wang, X. Zhang, H. Fu, X. Lv, F. Dong, G. Jiang, Hierarchical Pd/MnO2 nanosheet array supported on Ni foam: an advanced electrode for electrocatalytic hydrodechlorination reaction, Appl. Surf. Sci. 509 (2020), https://doi.org/10.1016/j.apsusc.2020.145369.
[29] Z. Fan, H. Zhao, K. Wang, W. Ran, J.F. Sun, J. Liu, R. Liu, Enhancing electrocatalytic hydrodechlorination through interfacial microenvironment modulation, Environ. Sci. Technol. (2023), https://doi.org/10.1021/acs.est.2c07462.
[30] M. Martin-Martinez, L.M. Gómez-Sainero, J. Bedia, A. Arevalo-Bastante, J. J. Rodriguez, Enhanced activity of carbon-supported Pd–Pt catalysts in the hydrodechlorination of dichloromethane, Appl. Catal. B: Environ. 184 (2016) 55–63, https://doi.org/10.1016/j.apcatb.2015.11.016.
[31] J. Wang, C. Cui, Y. Xin, Q. Zheng, X. Zhang, High-performance electrocatalytic hydrodechlorination of pentachlorophenol by amorphous Ru-loaded polypyrrole/foam nickel electrode, Electrochim. Acta 296 (2019) 874–881, https://doi.org/10.1016/j.electacta.2018.11.115.
[32] T. Liu, J. Luo, X. Meng, L. Yang, B. Liang, M. Liu, C. Liu, A. Wang, X. Liu, Y. Pei, J. Yuan, J. Crittenden, Electrocatalytic dechlorination of halogenated antibiotics via synergistic effect of chlorine-cobalt bond and atomic H, J. Hazard. Mater. 358 (2018) 294–301, https://doi.org/10.1016/j.jhazmat.2018.06.064.
[33] Y. Xu, X. Ding, H. Ma, Y. Chu, C. Ma, Selective hydrodechlorination of 3,5,6-trichloropicolinic acid at an activated silver cathode: synthesis of 3,5-dichloropicolinic acid, Electrochim. Acta 151 (2015) 284–288, https://doi.org/10.1016/j.electacta.2014.11.039.
[34] E. Verlato, W. He, A. Amrane, S. Barison, D. Floner, F. Fourcade, F. Geneste, M. Musiani, R. Seraglia, Preparation of silver-modified nickel foams by galvanic displacement and their use as cathodes for the reductive dechlorination of herbicides, ChemElectroChem 3 (2016) 2084–2092, https://doi.org/10.1002/celc.201600214.
[35] Y. Xu, Z. Yao, Z. Mao, M. Shi, X. Zhang, F. Cheng, H.B. Yang, H. b Tao, B. Liu, Single-Ni-atom catalyzes aqueous phase electrochemical reductive dechlorination reaction, Appl. Catal. B: Environ. 277 (2020), 119057, https://doi.org/10.1016/j.apcatb.2020.119057.
[36] Y. Chen, C. Feng, W. Wang, Z. Liu, J. Li, C. Liu, Y. Pan, Y. Liu, Electronic structure engineering of bimetallic Pd-Au alloy nanocatalysts for improving electrocatalytic hydrodechlorination performance, Sep. Purif. Technol. 289 (2022), https://doi.org/10.1016/j.seppur.2022.120731.
[37] L. Fang, C. Xu, W. Zhang, L.-Z. Huang, The important role of polyvinylpyrrolidone and Cu on enhancing dechlorination of 2,4-dichlorophenol by Cu/Fe nanoparticles: Performance and mechanism study, Appl. Surf. Sci. 435 (2018) 55–64, https://doi.org/10.1016/j.apsusc.2017.11.084.
[38] H. Tang, Z. Bian, Y. Peng, S. Li, H. Wang, Stepwise dechlorination of chlorinated alkenes on an Fe-Ni/rGO/Ni foam cathode: Product control by one-electron-transfer reactions, J. Hazard. Mater. 433 (2022), 128744, https://doi.org/10.1016/j.jhazmat.2022.128744.
[39] Z. Zhang, Y.B. Hu, W. Ruan, H. Ai, B. Yuan, M.L. Fu, Highly improved dechlorination of 2,4-dichlorophenol in aqueous solution by Fe/Ni nanoparticles supported by polystyrene resin, Chemosphere 266 (2021), 128976, https://doi.org/10.1016/j.chemosphere.2020.128976.
[40] H. Yu, S. Yang, B. Zhao, Y. Lu, S. Zhu, X. Wang, W. Qin, M. Huo, Enhanced electrochemical dechlorination of 4-chlorophenol on a nickel foam electrode modified with palladium, polypyrrole and graphene, J. Electroanal. Chem. 869 (2020), https://doi.org/10.1016/j.jelechem.2020.114099.
[41] L. Yang, Z. Chen, D. Cui, X. Luo, B. Liang, L. Yang, T. Liu, A. Wang, S. Luo, Ultrafine palladium nanoparticles supported on 3D self-supported Ni foam for cathodic dechlorination of florfenicol, Chem. Eng. J. 359 (2019) 894–901, https://doi.org/10.1016/j.cej.2018.11.099.
[42] K. Wang, S. Shu, M. Chen, J. Li, K. Zhou, J. Pan, X. Wang, X. Li, J. Sheng, F. Dong, G. Jiang, Pd-TiO2 Schottky heterojunction catalyst boost the electrocatalytic hydrodechlorination reaction, Chem. Eng. J. 381 (2020), 122673, https://doi.org/10.1016/j.cej.2019.122673.
[43] J. Li, C. Luan, Y. Cui, H. Zhang, L. Wang, H. Wang, Z. Zhang, B. Zhao, H. Zhang, X. Zhang, X. Cheng, Preparation and characterization of palladium/polyaniline/foamed nickel composite electrode for electrocatalytic dechlorination, Sep. Purif. Technol. 211 (2019) 198–206, https://doi.org/10.1016/j.seppur.2018.09.040.
[44] S. Song, Q. Liu, J. Fang, W. Yu, Enhanced electrocatalytic dechlorination of 2,4-dichlorophenoxyacetic acid on in situ prepared Pd-anchored Ni(OH)2 bifunctional electrodes: synergistic effect between H* formation on Ni(OH)2 and dechlorination steps on Pd, Catal. Sci. Technol. 9 (2019) 5130–5141, https://doi.org/10.1039/c9cy01359h.
[45] Y. Wu, L. Gan, S. Zhang, H. Song, C. Lu, W. Li, Z. Wang, B. Jiang, A. Li, Carbon-nanotube-doped Pd-Ni bimetallic three-dimensional electrode for electrocatalytic hydrodechlorination of 4-chlorophenol: enhanced activity and stability, J. Hazard. Mater. 356 (2018) 17–25, https://doi.org/10.1016/j.jhazmat.2018.05.034.
[46] J. Li, H. Wang, Z. Qi, C. Ma, Z. Zhang, B. Zhao, L. Wang, H. Zhang, Y. Chong, X. Chen, X. Cheng, D.D. Dionysiou, Kinetics and mechanisms of electrocatalytic hydrodechlorination of diclofenac on Pd-Ni/PPy-rGO/Ni electrodes, Appl. Catal. B: Environ. 268 (2020), 118696, https://doi.org/10.1016/j.apcatb.2020.118696.
[47] Z. Zhao, L. Yu, L. Zheng, T. Guo, Z. Lv, S. Song, H. Zheng, TiO2@PDA inorganic-organic core-shell skeleton supported Pd nanodots for enhanced electrocatalytic hydrodechlorination, J. Hazard. Mater. 435 (2022), 128998, https://doi.org/10.1016/j.jhazmat.2022.128998.
[48] J. Li, S. Ma, Z. Qi, J. Ding, M. Yin, B. Zhao, Z. Zhang, Y. Wang, H. Zhang, L. Wang, D.D. Dionysiou, Insights into the removal of chloramphenicol by electrochemical reduction on Pd/NiFe-MOF/foam-Ni electrode: performance and mechanism, Appl. Catal. B: Environ. 322 (2023), https://doi.org/10.1016/j.apcatb.2022.122076.
[49] D. Huang, D.J. Kim, K. Rigby, X. Zhou, X. Wu, A. Meese, J. Niu, E. Stavitski, J.-H. Kim, Elucidating the role of single-atom Pd for electrocatalytic hydrodechlorination, Environ. Sci. Technol. 55 (2021) 13306–13316, https://doi.org/10.1021/acs.est.1c04294.
[50] B.Y. Xia, H.B. Wu, X. Wang, X.W. Lou, Highly concave platinum nanoframes with high-index facets and enhanced electrocatalytic properties, Angew. Chem. Int. Ed. 52 (2013) 12337–12340, https://doi.org/10.1002/anie.201307518.
[51] J. Hutter, M. Iannuzzi, F. Schiffmann, J. VandeVondele, cp2k: atomistic simulations of condensed matter systems, WIREs Comput. Mol. Sci. 4 (2014) 15–25, https://doi.org/10.1002/wcms.1159.
[52] S. Gianluca, V. Angelo, I. Marcella, A.P. Carlo, P. Daniele, B. Alfons, , Modeling bulk and surface Pt using the “Gaussian and plane wave” density functional theory formalism: validation and comparison to k-point plane wave calculations, J. Chem. Phys. 129 (2008), 234703, https://doi.org/10.1063/1.3037227.
[53] U. Borštnik, J. VandeVondele, V. Weber, J. Hutter, Sparse matrix multiplication: the distributed block-compressed sparse row library, Parallel Comput. 40 (2014) 47–58, https://doi.org/10.1016/j.parco.2014.03.012.
[54] S. Grimme, J. Antony, S. Ehrlich, H. Krieg, A consistent and accurate ab initio parametrization of density functional dispersion correction (DFT-D) for the 94 elements H-Pu, J. Chem. Phys. 132 (2010), 154104, https://doi.org/10.1063/1.3382344.
[55] T. Lu, F. Chen, Multiwfn: a multifunctional wavefunction analyzer, J. Comput. Chem. 33 (2012) 580–592, https://doi.org/10.1002/jcc.22885.
[56] J. Xian, Q. Hua, Z. Jiang, Y. Ma, W. Huang, Size-dependent interaction of the poly (N-vinyl-2-pyrrolidone) capping ligand with Pd nanocrystals, Langmuir 28 (2012) 6736–6741, https://doi.org/10.1021/la300786w.
[57] H. Zhu, X. Song, X. Han, X. Zhang, J. Bao, N. Zhang, G. He, Co3O4 nanosheets preferentially growing (220) facet with a large amount of surface chemisorbed oxygen for efficient oxidation of elemental mercury from flue gas, Environ. Sci. Technol. 54 (2020) 8601–8611, https://doi.org/10.1021/acs.est.0c03427.
[58] H.C. Peng, S. Xie, J. Park, X. Xia, Y. Xia, Quantitative analysis of the coverage density of Br- ions on Pd{100} facets and its role in controlling the shape of Pd nanocrystals, J. Am. Chem. Soc. 135 (2013) 3780–3783, https://doi.org/10.1021/ja400301k.
[59] Y. Peng, M. Cui, Z. Zhang, S. Shu, X. Shi, J.T. Brosnahan, C. Liu, Y. Zhang, P. Godbold, X. Zhang, F. Dong, G. Jiang, S. Zhang, Bimetallic composition-promoted electrocatalytic hydrodechlorination reaction on silver–palladium alloy nanoparticles, ACS Catal. 9 (2019) 10803–10811, https://doi.org/10.1021/acscatal.9b02282.
[60] W. Fu, S. Shu, J. Li, X. Shi, X. Lv, Y.-X. Huang, F. Dong, G. Jiang, Identifying the rate-determining step of the electrocatalytic hydrodechlorination reaction on palladium nanoparticles, Nanoscale 11 (2019) 15892–15899, https://doi.org/10.1039/c9nr04634h.